ASM Handbook®

Formerly Ninth Edition, Metals Handbook

Volume 9
Metallography and Microstructures

Prepared under the direction of
the ASM Handbook Committee

Kathleen Mills, Manager of Editorial Operations
Joseph R. Davis, Senior Technical Editor
James D. Destefani, Technical Editor
Deborah A. Dieterich, Production Editor
George M. Crankovic, Assistant Editor
Heather J. Frissell, Assistant Editor
Diane M. Jenkins, Word Processing Specialist

William H. Cubberly, Director of Publications
Robert L. Stedfeld, Assistant Director of Publications

Editorial Assistance
Robert T. Kiepura
Bonnie R. Sanders

ASM INTERNATIONAL®
The Materials Information Society

Quantitative Metallography

By Ervin E. Underwood
Professor of Metallurgy
Fracture and Fatigue Research Laboratory
School of Materials Engineering
Georgia Institute of Technology

QUANTITATIVE METALLOGRAPHY (or, more generally, stereology) deals with the quantitative relationships between measurements made on the two-dimensional plane of polish and the magnitudes of the microstructural features in the three-dimensional metal or alloy. As material specifications become stricter and performance limits are narrowed, it becomes necessary to specify and control microstructure quantitatively. This article will review the important equations, the basic measurements, and the applications of these methods to pure metals alloys. Additional information on quantitative metallography, including the use of automatic image analyzers for determining microstructural characteristics, can be found in the article "Color Metallography" in this Volume.

Table 1 shows the principal symbols used and gives examples of the combined notation in common usage (Ref 1). The term S_V, for example, refers to surface area per unit volume and represents the fraction S/V_T, in which the numerator is the microstructural feature and the denominator (total test volume) is a test quantity. Each symbol represents a geometrical element and a specific dimension. Therefore, the dimensionality of the combined terms and equations is readily apparent and consistent.

Basic Measurements

Of greatest interest are the simple counting measurements, P_P, P_L, N_L, P_A, and N_A, because of the ease and speed with which these data can be gathered. Several theoretical analyses have elucidated efficient sampling techniques. With one technique, it is possible to predict the number of measurements required to achieve the desired accuracy (Ref 2). This has been applied to the point-count method, which refers to the number of test points that fall in some selected areal feature of the microstructure (such as α phase) on the plane of polish.

The number of points, P_α, that fall in the α phase divided by P_T, the total number of test points, gives the ratio P_α/P_T, or P_P. Those grid points that appear to fall on a boundary can be counted as one half. This gives the operator a guide to the magnitude of the experimental error.

Figure 1 shows one type of point-count grid (Ref 3) with the test points at the intersections. Figures 2 and 3 show examples of point grids selected for optimum results, depending on the type of microstructure to which they are applied. Note that on average not more than one grid point falls in any second-phase area and that the grid spacing selected is close to the diameter of the second-phase particles. A grid can be inserted in the eyepiece of the microscope, or a grid marked on clear plastic can be used with a photomicrograph or a projection screen. For best operator efficiency in counting, it is useful to

Table 1 Principal symbols and combined notations for quantitative metallography

Symbol	Units	Description	Common name
P	...	Number of point elements or test points	...
P_P	...	Point fraction (number of point elements per total number of test points)	Point count
L	mm	Length of linear elements or test line length	...
P_L	mm^{-1}	Number of point intersections per unit length of test line	...
L_L	mm/mm	Sum of linear intercept lengths divided by total test line length	Lineal fraction
A	mm^2	Planar area of intercepted features or test area	...
S	mm^2	Surface area or interface area, generally reserved for curved surfaces	...
V	mm^3	Volume of three-dimensional structural elements or test volume	...
A_A	mm^2/mm^2	Sum of areas of intercepted features divided by total test area	Areal fraction
S_V	mm^2/mm^3	Surface or interface area divided by total test volume (surface-to-volume ratio)	...
V_V	mm^3/mm^3	Sum of volumes of structural features divided by total test volume	Volume fraction
N	...	Number of features	...
N_L	mm^{-1}	Number of interceptions of features divided by total test line length	Lineal density
P_A	mm^{-2}	Number of point features divided by total test area	...
L_A	mm/mm^2	Sum of lengths of linear features divided by total test area	Perimeter (total)
N_A	mm^{-2}	Number of interceptions of features divided by total test area	Areal density
L_V	mm/mm^3	Length of features per test volume	...
N_V	mm^{-3}	Number of features per test volume	Volumetric density
$\bar{L}$	mm	Mean linear intercept distance, L_L/N_L	...
$\bar{A}$	mm^2	Mean areal intercept, A_A/N_A	...
$\bar{S}$	mm^2	Mean particle surface area, S_V/N_V	...
$\bar{V}$	mm^3	Mean particle volume, V_V/N_V	...

Note: Fractional parameters are expressed per unit length, area, or volume
Source: Ref 1

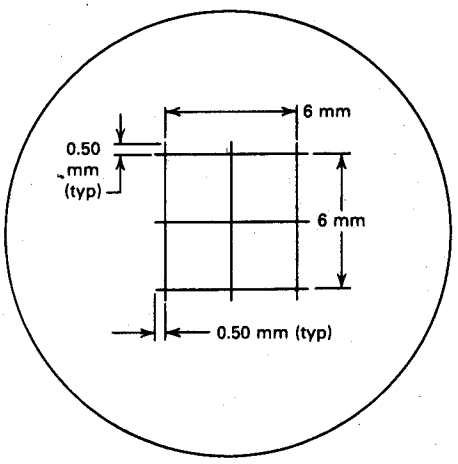

Fig. 1 Typical point-count grid. Figures 2 and 3 show applications. (Ref 3)

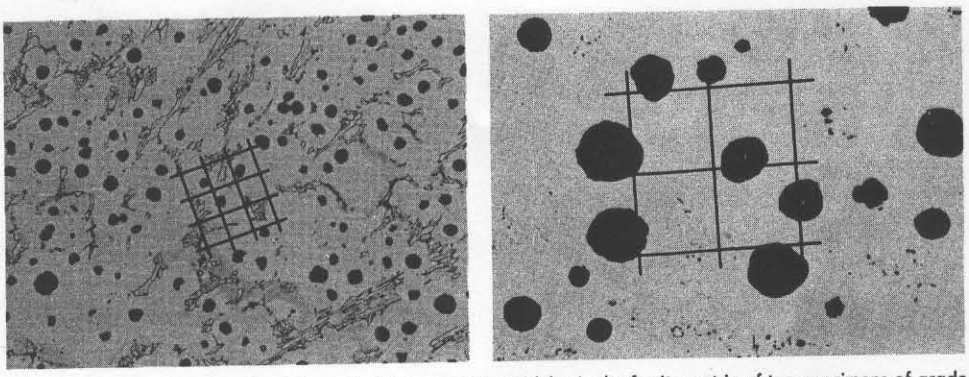

Fig. 2, 3 Application of point-count grids to graphite nodules in the ferrite matrix of two specimens of grade 60-45-12 ductile iron. Fig. 2: 2% nital. 100×. Fig. 3: 2% nital, lightly etched. 140×

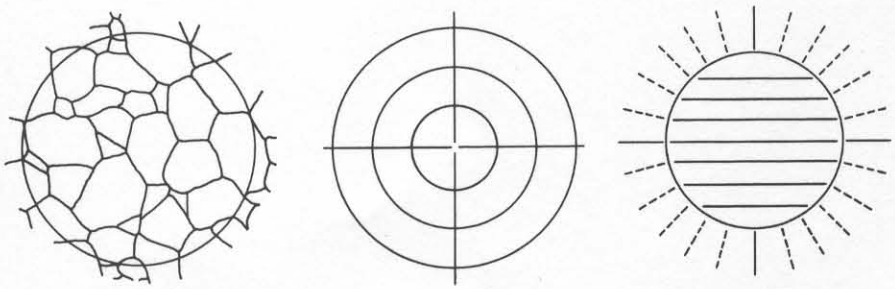

(a) (b)

Fig. 4 (a) Grain-boundary traces in a typical single-phase alloy (Ref 4). (b) Circular (left) and parallel (right) linear test grids for P_L counts. Both types of grids may be used for measuring random structures like that shown in (a); the grid at right is applicable to oriented structures such as the one shown in Fig. 5. (Ref 1)

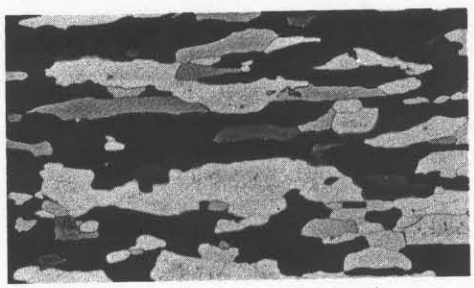

Fig. 5 Elongated grain-boundary traces in extruded molybdenum; typical of oriented structures measured with the grid at the right in Fig. 4(b). Etchant and magnification not reported

limit the number of hits on any one application of the grid to five or six. Therefore, a 3 by 3, 4 by 4, or 5 by 5 point grid suffices for most applications, because the magnification can be adjusted for a particular microstructure.

Another important measurement frequently required in quantitative microstructural analysis is the number of points of intersection generated per unit length of test lines, P_L. A test line or linear array is applied randomly to a microstructure containing linear features, such as the structure drawn in Fig. 4(a). The points of intersection along the test lines are counted as they are placed at several positions and angles over the entire microstructure until enough intersections have been counted. Figure 4(b) shows examples of circular and parallel linear test grids for P_L counts (Ref 1). Both grids in Fig. 4(b) may be used for random microstructures (such as the one in Fig. 4a); the grid with radii spaced at 15° angular intervals finds application for directional measurements on oriented structures, such as the one shown in Fig. 5. The total lengths of the circular and parallel linear test grids are determined in advance to facilitate subsequent calculations.

Other basic measurements that involve counting are N_L, P_A, and N_A. N_L corresponds closely to P_L, except that N_L is reserved for objects (such as particles) instead of points (for example, the intersections of grain-boundary traces by test lines). N_L is defined as the number of interceptions of particles per unit length of test line. This definition allows for the possibility that a particle with an irregular outline may be intercepted more than once by the same test line. Therefore, the relationships $P_L = N_L$, for space-filling grains, and $P_L = 2N_L$, for isolated particles, regardless of their shape, are maintained.

P_A and N_A are also related. P_A refers to points per unit area, and N_A to objects per unit area (see the nodules in Fig. 2). If the grain junctions (triple points) in Fig. 4(a) are counted as points, $P = 59$, and for a test area A_T within the circle equal to 0.5 mm², $P_A = 59/0.5 = 118$ mm^{-2}. A count of the grains in Fig. 4(a) gives a value of $N = 30.5$ (counting border grains intercepted by the circular perimeter as one half a grain each). Therefore, $N_A = 30.5/0.5 = 61$ mm^{-2}.

When counting objects or points within an area, care must be taken that none is overlooked or counted twice. An open square grid superimposed over the photomicrograph or microstructure is used frequently to ensure accurate counting. Figure 6 gives an example of using a simple grain count to plot elongation and tensile strength as functions of the number of grains, N, in the cross sections of the specimens (Ref 5).

Two procedures using combined measurements are described below. The older method (Ref 6) was proposed to obtain the surface-to-volume ratio of discrete particles. The particles are embedded in a suitable material, then sectioned. In principle, short test lines of length l are "thrown" randomly on the microstructure, as shown in Fig. 7(a). Two types of points are counted: points of intersection with the boundaries, P, and the end points that hit within the second-phase areas, h. For particles of α phase, the equation is:

$$\frac{S_\alpha}{V_\alpha} = \frac{4P}{hl} \qquad \text{(Eq 1)}$$

where the mean particle surface area, S_α, refers to the mean particle volume, V_α, not an arbitrary test volume. Figure 7(a) illustrates various counting possibilities, which, for a test line $l = 0.02$ mm, gives $S_\alpha/V_\alpha = (4 \times 7)/(5 \times 0.02) = 280$ mm^{-1}. Figure 7(b) reproduces an excellent grid for these combined measurements (Ref 7).

A combined method for obtaining the S/V ratio of discrete particles has also been proposed (Ref 8). Both a point count, P_P, and an intersection count, P_L, are made simultaneously using a superimposed square grid, as depicted in Fig. 8. The equation for individual, isolated particles is:

$$\frac{S_\alpha}{V_\alpha} = \frac{2P_L}{P_P} \qquad \text{(Eq 2)}$$

For a system of particles in a matrix, the equation is:

$$\frac{(S_V)_\alpha}{(V_V)_\alpha} = \frac{2P_L}{P_P} \qquad \text{(Eq 3)}$$

Assuming the numbers shown for the individual particles in Fig. 8 represent average values obtained after several random placements of the grid and that the total unmagni-

Table 2 Relationship of measured (○) and calculated (□) quantities

Dimensions arbitrarily expressed in millimeters

Microstructural feature	Dimensions of symbols: mm^0	mm^{-1}	mm^{-2}
Points	P_P	P_L →	P_A
Lines	L_L	L_A	L_V
Surfaces	A_A	S_V ↗	
Volumes	V_V		

Basic equations

$V_V = A_A = L_L = P_P$ (mm^0) (Eq 4)

$S_V = (4/\pi)\, L_A = 2P_L$ (mm^{-1}) (Eq 5)

$L_V = 2P_A$ (mm^{-2}) (Eq 6)

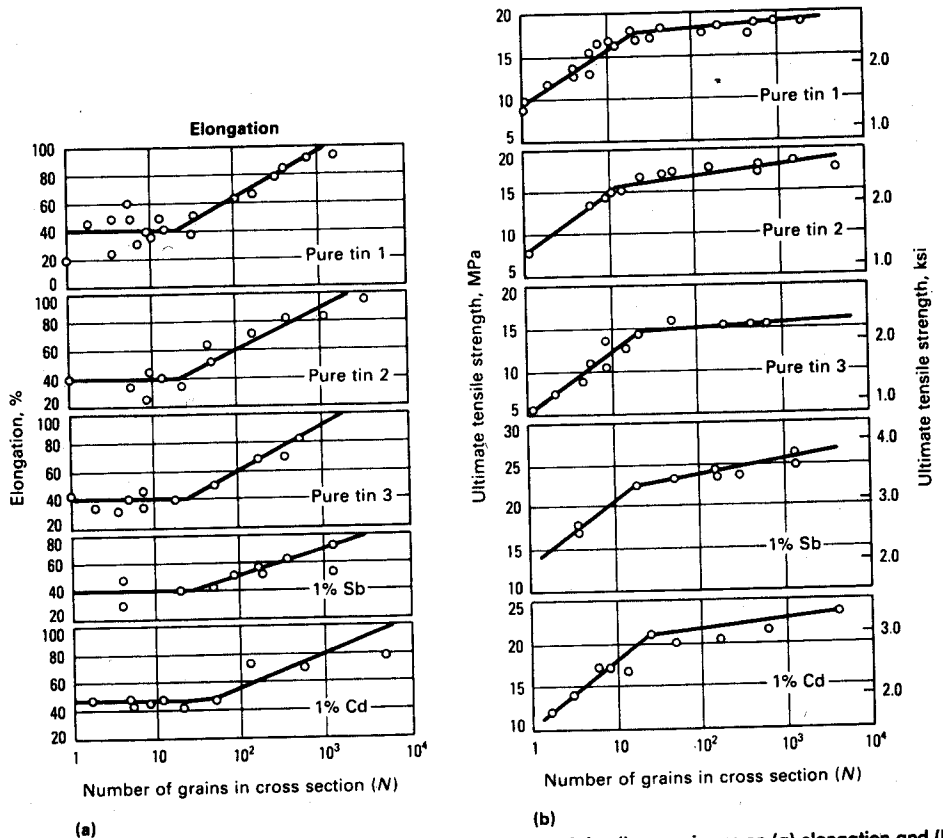

Fig. 6 Effect of number of grains (N) in cross sections of tin and tin alloy specimens on (a) elongation and (b) ultimate tensile strength. (Ref 5)

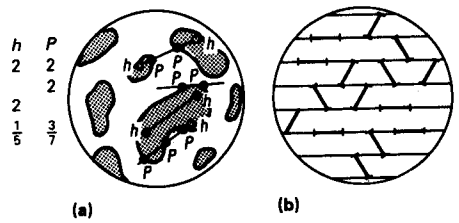

Fig. 7 (a) Chalkley method for determining the surface-to-volume ratio of discrete particles. (b) A grid for combined point and intersection count. (Ref 7)

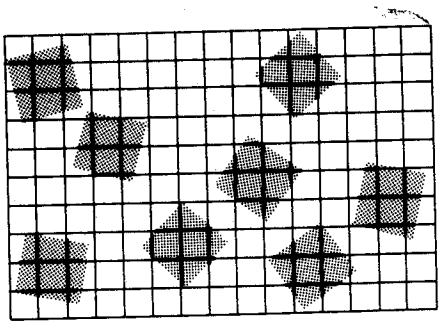

Fig. 9 Equivalence of areal, linear, and point ratios, $A_A = L_L = P_P$. (Ref 1)

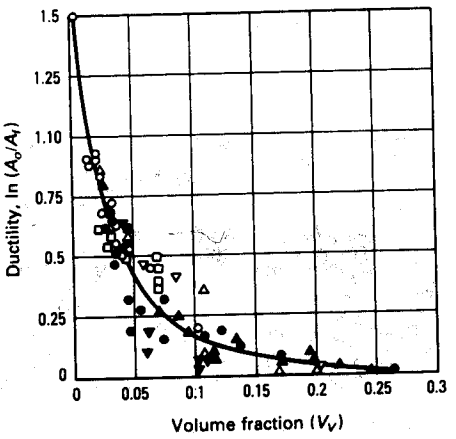

Fig. 10 Relationship between ductility and the volume fraction of various dispersions in copper. (Ref 12)

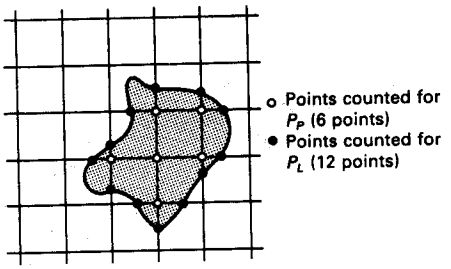

Fig. 8 Superimposed square grid used in the Saltykov method for determining the surface-to-volume ratio of discrete particles. P_P represents a point count and P_L represents an intersection count. (Ref 1)

fied grid length is 1 mm, then $S/V = (2 \times 12)/(6/36) = 144\ \text{mm}^{-1}$.

Basic Equations

The basic equations for points, lines, surfaces, and volumes in a microstructure are well known and well documented (Ref 1, 3, 8-11). Consequently, derivations will not be given here. Instead, practical applications to actual microstructures will be stressed.

Table 2 shows the interrelationships between microstructural features that can and cannot be measured (Ref 1). Arrows indicate those quantities that yield the normally inaccessible three-dimensional quantities V_V, S_V, and L_V. Below the triangular matrix are written the corresponding basic equations.

Equation 4 in Table 2 states the equality of volume fraction to the areal ratio, linear ratio, and point ratio of the selected phase as seen on random sections through the microstructure. The measurement of volume fraction is usually most efficiently performed with the point count, as illustrated in Fig. 1 to 3. Under unusual circumstances, areal ratios can be obtained with a planimeter; linear ratios are commonly measured by means of a Hurlbut counter. Quantitative TV-scanning equipment is being used increasingly for routine applications in which large numbers of specimens make automation economically feasible.

Figure 9 shows the interrelationship of areal, length, and point measurements through the equations $A_A = L_L = P_P$ (Ref 1). The volume fraction is used frequently in studies of metallurgical systems and phenomena. Figure 10 depicts the relationship between ductility and the volume fraction of various dispersions in copper (Ref 12), and Fig. 11 illustrates the application of volume-fraction measurements to establish the phase boundaries of a two-phase field (Ref 13).

Equation 5 in Table 2 combines two important equations, both of which require a P_L measurement:

$$S_V = 2P_L \qquad \text{(Eq 5a)}$$

$$L_A = \frac{\pi}{2} P_L \qquad \text{(Eq 5b)}$$

When surface area per unit volume is required, Eq 5(a) is used. For example, total

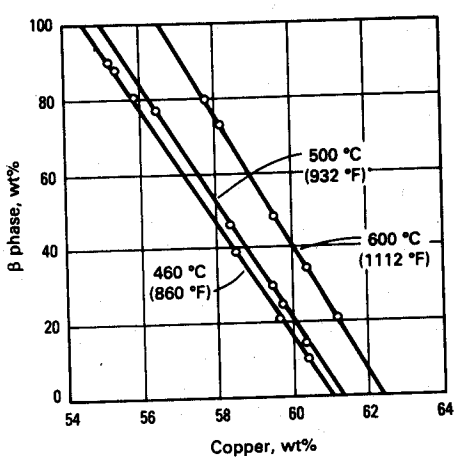

Fig. 11 Application of volume-fraction measurements to establish the phase boundaries of a two-phase field. (Ref 13)

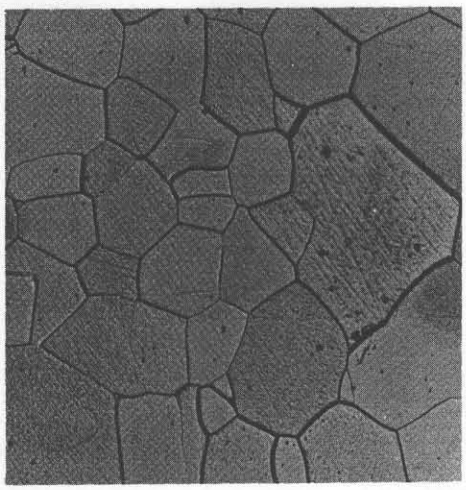

Fig. 12 Grain-boundary traces outlining the recrystallized grains of a single-phase palladium solid solution. 10% KCN + 10% $(NH_4)_2S_2O_8$. 75×

grain-boundary surface area in a single-phase alloy (Fig. 12) may be desired. Also, S_V could be used for analyzing grain-boundary precipitates (Fig. 13 to 15), for transformation products growing out of grain boundaries (Fig. 16), or for obtaining the interphase boundary area in a eutectic alloy (Fig. 17).

When linear traces in the plane of polish are of interest, L_A is the parameter of choice, and Eq 5(b) would be used. In corrosion studies, for example, the pertinent feature is the length of grain-boundary traces exposed to the corroding medium. In other studies, the microstructural feature may be considered essentially linear, such as the thin twins in Fig. 18. Here, in a P_L traverse, each twin intersected would be counted only once. Using the circular grid around the hardness impression, curves of L_A versus strain can be calculated, as shown in Fig. 19. For other twins, however, the total twin-matrix interface length may be required. The interfaces on each side of the twinned regions would be counted separately, as in Fig. 20, and each time the twin was intersected by the test line, it would count as two.

In Eq 6, for line length per unit volume ($L_V = 2P_A$), the points counted are those in the test area caused by the intersections of the test plane with the linear elements of the microstructure. Equation 6 usually requires only one test plane for linear elements that are randomly oriented in space. However, randomness in the microstructure is not essential to Eq 6, because random sampling can be ensured by selecting a random orientation of the plane of polish.

Typical examples of linear elements in microstructures are dislocation lines, grain edges where three adjacent grains contact, needlelike precipitate particles, and slag or oxide stringers. Figure 21 shows dislocation etch pits, which are counted (P_A) to get the dislocation density (L_V). Figures 4(a) and 12 represent single-phase materials with the grain edges revealed at the junctions of grain-boundary traces. These triple points are counted (P_A) to find the length of grain-boundary edges (L_V). Figure 22 shows elongated, essentially linear, nonmetallic inclusions that can also be analyzed according to Eq 6.

Oriented Structures

Although the basic equations (Eq 4 to 6) apply to any microstructure, special equations are available for special types of microstructures (Ref 1). For example, oriented systems of lines or surfaces may be encountered, and the directional characteristics, in addition to the mean values, may be desired. In such cases, transverse or longitudinal sections or both are used instead of random sections.

Next, systems of oriented lines in a two-dimensional plane, systems of oriented lines in three-dimensional space, and systems of oriented surfaces in three-dimensional space are discussed. The oriented systems can also be described as completely oriented systems, in which all elements are parallel, or as partially oriented systems, in which random and oriented elements occur. In both cases, however, orientation directions are clearly defined and recognizable; in fact, several orientation systems can exist in the same microstructure, each with its own orientation direction or plane.

Examples of systems of oriented lines in a plane are provided by twin traces in the plane of polish (Fig. 20), dislocation lines in the surface of a silicon crystal (Fig. 23), and grain-boundary traces in extruded molybdenum (Fig. 5).

The three equations applicable to these partially oriented systems of lines in a plane refer to the random (ran) and oriented (or) portions of the system of lines as well as to the total (tot) length per unit area. They are:

$$(L_A)_{ran} = 1.571(P_L)_{\parallel} \quad \text{(Eq 7a)}$$

$$(L_A)_{or} = (P_L)_{\perp} - (P_L)_{\parallel} \quad \text{(Eq 7b)}$$

$$(L_A)_{tot} = (P_L)_{\perp} + 0.571(P_L)_{\parallel} \quad \text{(Eq 7c)}$$

where the $(P_L)_{\perp}$ and $(P_L)_{\parallel}$ measurements are made with test lines perpendicular and parallel to the orientation direction, respectively. Note that $(L_A)_{tot} = (L_A)_{ran} + (L_A)_{or}$. Of course, if the system of lines is completely oriented, $(P_L)_{\parallel}$ will be zero and $(L_A)_{or} = (L_A)_{tot} = (P_L)_{\perp}$.

The twin traces in Fig. 24 represent a system of lines in a plane with essentially four orientation directions. A grid of parallel test lines (such as the one at right in Fig. 4b) is applied perpendicular to each orientation direction, in turn, and the intersections with the twins perpendicular to the test lines are counted. If the twin traces are assumed to be completely oriented, then $(L_A)_{or} = (P_L)_{\perp}$, and the line length is obtained directly for each orientation direction as a function of angle from a reference line. Figure 25 summarizes the results obtained in this way.

Many common microstructures have features that can be described as a system of oriented lines in space (that is, throughout the alloy). Examples are elongated nonmetal-

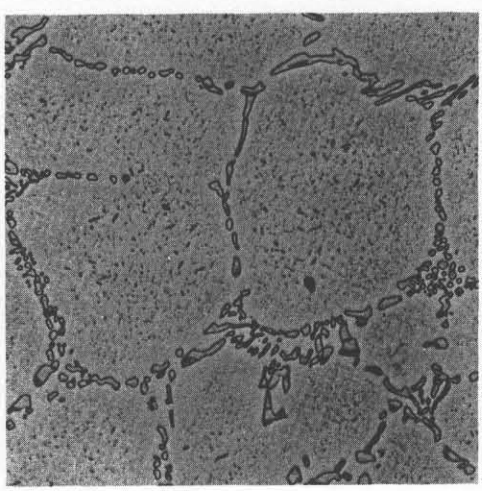

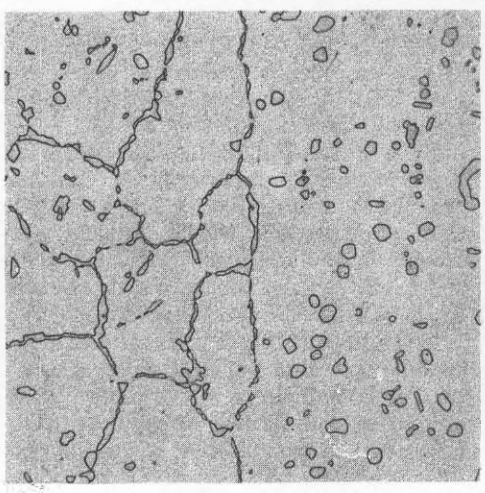

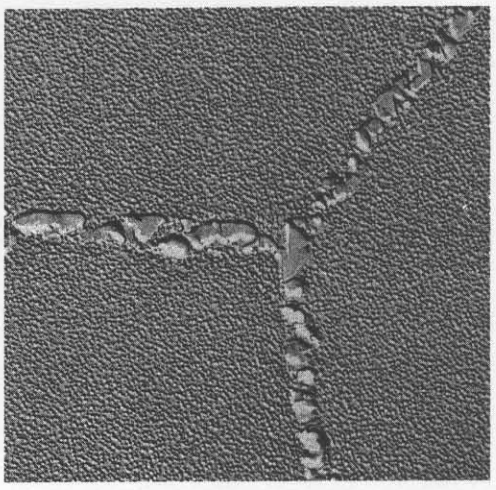

Fig. 13, 14, 15 Precipitated particles in grain boundaries of three heat-resistant alloys. Fig. 13: Fe-35Ni-16Cr casting alloy. Hot alkaline potassium ferricyanide. 250×. Fig. 14: RA 333, a wrought nickel-base alloy. 25 mL HCl, 10 mL methanol, 7 mL HNO_3. 250×. Fig. 15: Waspaloy, also a wrought nickel-base alloy. Electrolytic etch, H_2SO_4, H_3PO_4, HNO_3. 10 000×

lic inclusions (Fig. 22), parallel rods in unidirectionally solidified eutectics (Fig. 26), and oriented dislocation arrays (Fig. 27 to 29), all of which show pronounced linear directional characteristics.

For a partially oriented system of lines in the alloy:

$$(L_V)_{ran} = 2(P_A)_{\parallel} \quad \text{(Eq 8a)}$$

$$(L_V)_{or} = (P_A)_{\perp} - (P_A)_{\parallel} \quad \text{(Eq 8b)}$$

$$(L_V)_{tot} = (P_A)_{\perp} + (P_A)_{\parallel} \quad \text{(Eq 8c)}$$

where $(P_A)_{\perp}$ and $(P_A)_{\parallel}$ refer to measurements of point density on planes perpendicular and parallel to the orientation direction, respectively. If the system of lines is completely oriented, $(P_A)_{\parallel}$ is zero, and $(L_V)_{or} = (P_A)_{\perp}$. Although some microstructural features are not truly linear, they can be considered so for practical purposes if they have sufficient linearity. Of course, if the cross-sectional thickness is too great, the $(P_A)_{\parallel}$ measurements will be difficult to make.

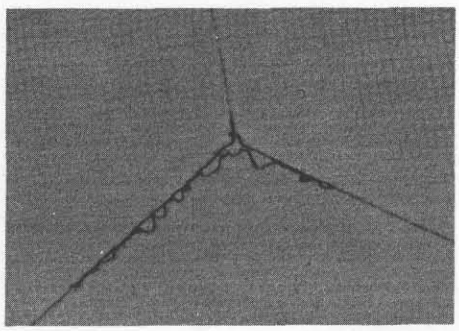

Fig. 16 Particles of Fe_3C nucleating at grain boundaries of secondary-recrystallized 3.25% silicon steel strip. Nital. 1000×

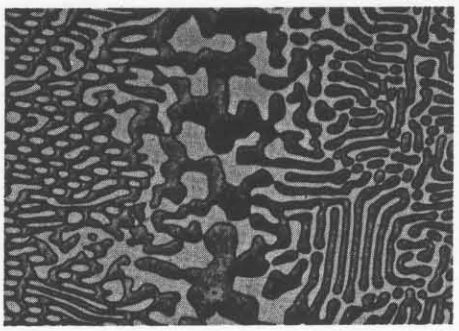

Fig. 17 Interfaces between phases in a reversible-matrix, aluminum-copper eutectic alloy. Etchant and magnification not reported

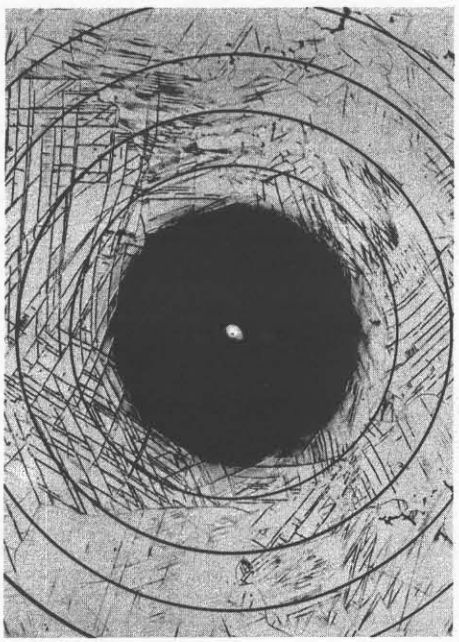

Fig. 18 Circular grid superimposed on a micrograph, showing twinning around a hardness impression in as-cast Mo-12.5Os alloy. See also Fig. 19. Etchant and magnification not reported. (Ref 14)

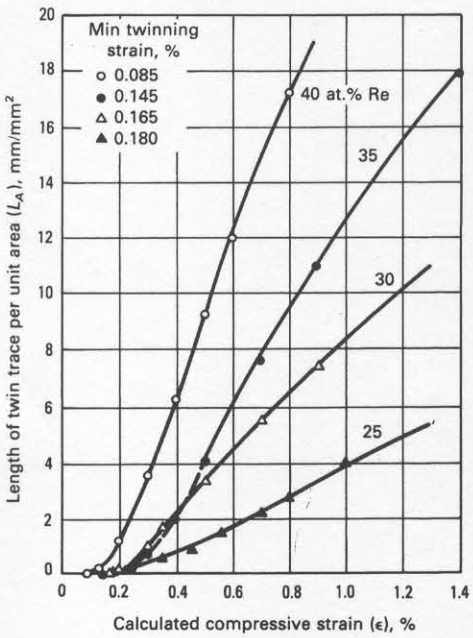

Fig. 19 Application of data obtained with the aid of circular grids around hardness impressions to calculation of compressive strain in cast chromium-base alloys containing various amounts of rhenium. (Ref 14)

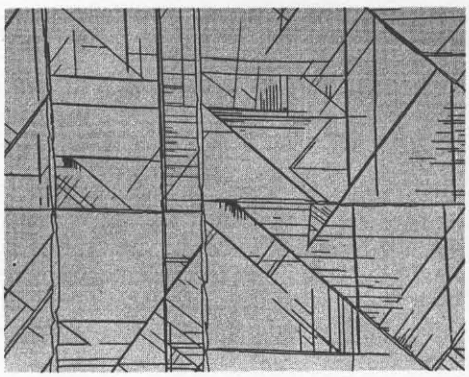

Fig. 20 Twinned structure in a lightly etched Mo-35Re single crystal. Etchant and magnification not reported

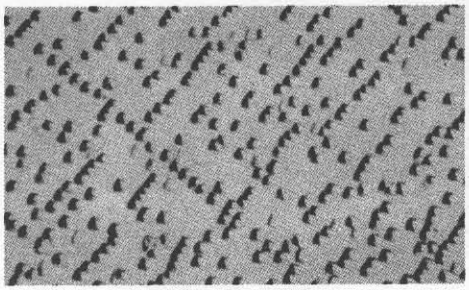

Fig. 21 Etch pits due to dislocation lines in copper. Etchant and magnification not reported. (Ref 15)

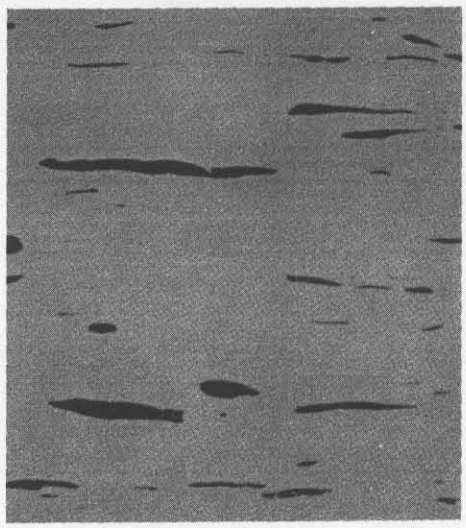

Fig. 22 Elongated sulfide inclusions in free-cutting type 303 stainless steel bar (0.25% S). Longitudinal section. As-polished. 250×

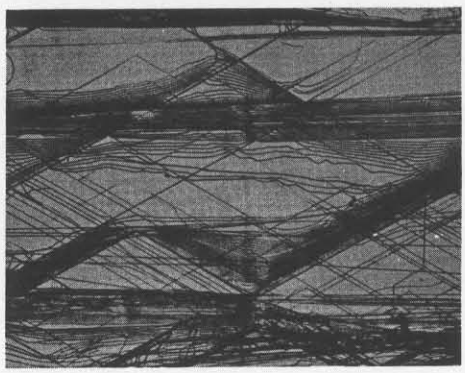

Fig. 23 Dislocation lines in (111) surface of silicon crystal. Etchant and magnification not reported. (Ref 16)

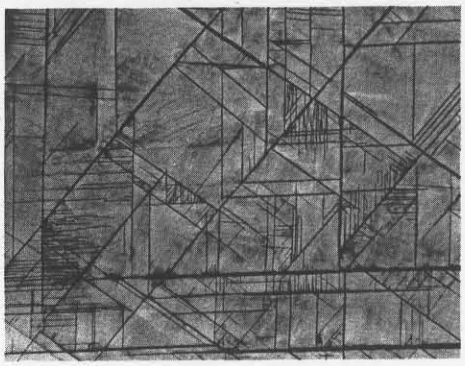

Fig. 24 Twinned structure in a heavily etched Mo-35Re single crystal. Etchant and magnification not reported

Another major type of oriented structure consists of surfaces in the alloy. Examples of oriented planar features in the microstructure are pearlites in steel (Fig. 30), lamellae in unidirectionally solidified eutectics (Fig. 31), and lamellar precipitates observed by thin-foil electron transmission microscopy (Fig. 32).

These oriented surfaces are subclassified as planar orientation, because the planar surfaces are essentially parallel to an orientation plane (or planes). The three equations applicable to a partially oriented system of surfaces with planar orientation are:

$$(S_V)_{ran} = 2(P_L)_{\parallel} \quad \text{(Eq 9a)}$$

$$(S_V)_{or} = (P_L)_{\perp} - (P_L)_{\parallel} \quad \text{(Eq 9b)}$$

$$(S_V)_{tot} = (P_L)_{\perp} + (P_L)_{\parallel} \quad \text{(Eq 9c)}$$

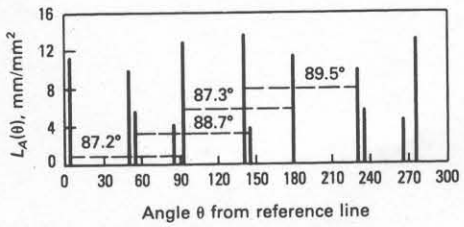

Fig. 25 Twin-trace length as a function of angle for the structure shown in Fig. 24. (Ref 14)

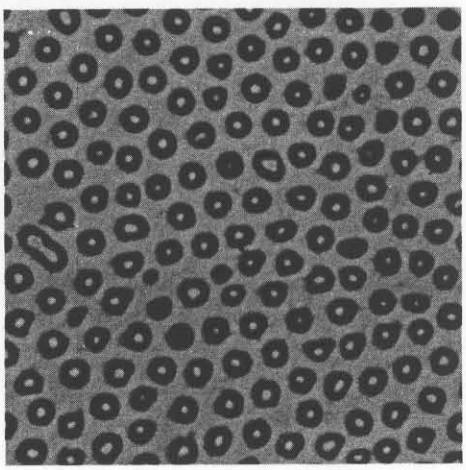

Fig. 26 Transverse section through parallel rods in a unidirectionally solidified Mg-32Al eutectic alloy. Growth rate was 1.5×10^{-2} mm/s (6×10^{-4} in./s). Temperature gradient was 3.7 °C/mm (1.7 °F/10^{-2}in.). Etchant and magnification not reported. (Ref 17)

where $(P_L)_{\perp}$ and $(P_L)_{\parallel}$ are measurements made perpendicular and parallel to the orientation plane, respectively. If the system of surfaces is completely oriented, as in portions of Fig. 32, $(P_L)_{\parallel}$ is zero, and $(S_V)_{or} = (P_L)_{\perp}$.

A sequence of extruded beryllium specimens with different initial powder sizes exemplifies the analysis of a system of partially oriented surfaces (Ref 1). The essential data are as follows:

Specimen	Initial powder size, mm	$(P_L)_{\perp}$, mm^{-1}	$(P_L)_{\parallel}$ mm^{-1}
1	0.004	164.8	115.0
2	0.100	104.2	69.5
3	0.250	69.0	56.8

Assuming planar orientation, substitution in Eq 9(b) and 9(c) shows that for specimens 1, 2, and 3, respectively:

$$(S_V)_{or} = (P_L)_{\perp} - (P_L)_{\parallel}$$
$$= 164.8 - 115.0 = 49.8 \text{ mm}^{-1}$$
$$= 104.2 - 69.5 = 34.7 \text{ mm}^{-1}$$
$$= 69.0 - 56.8 = 12.2 \text{ mm}^{-1}$$

and

$$(S_V)_{tot} = (P_{L)\perp} + (P_{L)\parallel}$$
$$= 164.8 + 115.0 = 279.8 \text{ mm}^{-1}$$
$$= 104.2 + 69.5 = 173.7 \text{ mm}^{-1}$$
$$= 69.0 + 56.8 = 125.8 \text{ mm}^{-1}$$

The fractional, or percentage, amount of planar orientation, represented by Ω_{pl} is $(S_V)_{or}/(S_V)_{tot}$, or:

$$\Omega_{pl} = \frac{49.8}{279.8} = 17.8\%$$
$$= \frac{34.7}{173.7} = 20.0\%$$
$$= \frac{12.2}{125.8} = 9.7\%$$

for specimens 1, 2, and 3, respectively. The results suggest that some mechanical properties may fall out of sequence even though the mean grain intercept length (equal to the reciprocal of P_L) varies directly with the initial powder size.

Where the grains (or particles, inclusions, or precipitates) are markedly elongated, a shape index may prove useful. One of the simplest indices to express elongation is the ratio of mean length to mean width:

$$Q = \frac{D_{\parallel}}{D_{\perp}} = \frac{(P_L)_{\perp}}{(P_L)_{\parallel}} \quad \text{(Eq 10)}$$

Using the data given above for extruded beryllium specimens, Eq 10 becomes:

$$Q = \frac{(P_L)_{\perp}}{(P_L)_{\parallel}}$$
$$= \frac{164.8}{115.0} = 1.43$$
$$= \frac{104.2}{69.5} = 1.50$$
$$= \frac{69.0}{56.8} = 1.21$$

for specimens 1, 2, and 3, respectively. For equiaxed grains, of course, Q-ratios closer to unity would be expected.

Lamellar structures perhaps most typically exemplify oriented surfaces. A measure of the fineness of lamellae (as in pearlite, for example) is the so-called interlamellar or true spacing, S_o, defined as the perpendicular distance across a single pair of contiguous lamellae. Because the true spacing is difficult to determine directly, the mean random spacing, σ, defined as:

$$\sigma = \frac{1}{N_L} \quad \text{(Eq 11)}$$

where N_L is the number of alternate lamellae intersected per unit length of random test lines, is measured instead. The true spacing can then be found according to Eq 12, which has been confirmed experimentally:

$$S_o = \frac{\sigma}{2} \quad \text{(Eq 12)}$$

Figure 33 illustrates three types of spacings and three types of distances. Spacings are essentially center-to-center lengths; distances, edge-to-edge lengths. The interlamellar distances are related to the spacings through the linear intercept ratio (L_L) as in:

$$\lambda = (L_L)\sigma \quad \text{(Eq 13)}$$

or by the mean intercept length (L_3) as in:

$$L_3 = \sigma - \lambda \quad \text{(Eq 14)}$$

Fig. 27, 28, 29 Oriented dislocation arrays in thin foils. Fig. 27: copper. (Ref 15). Fig. 28: iron. (Ref 15). Fig. 29: Armco iron. (Ref 18). Etchants and magnifications not reported

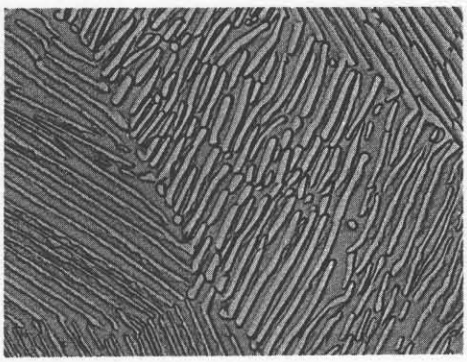

Fig. 30 Replica electron micrograph showing lamellar pearlite in a 1090 hot-rolled steel bar. Picral. 2000×

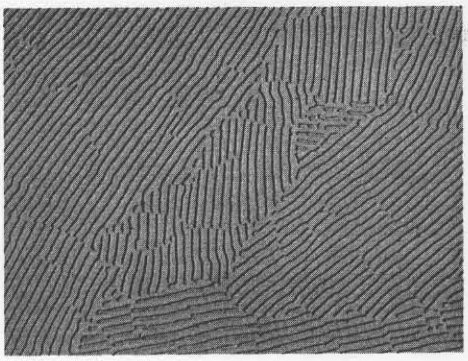

Fig. 31 Lamellae in a unidirectionally solidified aluminum-copper eutectic alloy. Etchant and magnification not reported. (Ref 1)

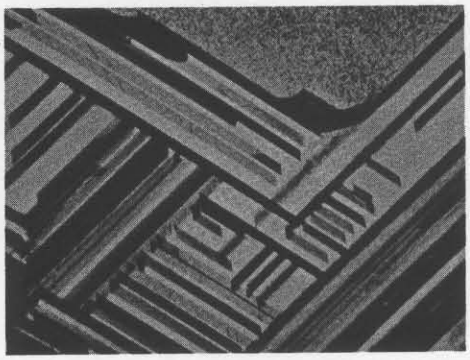

Fig. 32 Thin-foil transmission electron micrograph showing lamellar precipitate in Fe-30Ni-6Ti alloy. Magnification not reported. (R.C. Glenn)

The subscript 3 refers to the three-dimensionality of the parameter. Finally, it is noted that:

$$S_V = \frac{4}{\sigma} \qquad \text{(Eq 15)}$$

where S_V is the lamellar interface area per unit volume.

Grain Size

Grain sizes, or diameters, have been determined by several methods. Because the grains normally found in alloys have irregular shapes, the definition of a diameter is usually arbitrary.

Fortunately, a general, quantitative length parameter provides a unique, assumption-free value for any granular, space-filling structure, regardless of grain shape, size, or position. This length parameter is the mean intercept length L_3 obtained from simple L_2 intercept measurements on the plane of polish. For many random planes, of course, the averaged L_2 values become the true, three-dimensional L_3 parameter.

For space-filling grains, the mean intercept length is defined as:

$$L_3 = \frac{1}{N_L} = \frac{L_T}{PM} \qquad \text{(Eq 16)}$$

where N_L has been described above. In essence, L_3 equals the total test-line length, L_T, divided by the magnification, M, and the number of grain-boundary intersections, P (P equals N for space-filling grains).

When L_3 is expressed in millimeters, it gives the same value as the intercept procedure described in ASTM specification E 112 (Ref 4). This specification also is the basis for the ASTM grain-size number N, defined as:

$$N = \frac{\log n}{\log 2} + 1.0000 \qquad \text{(Eq 17)}$$

where n is the number of grains per square inch at 100× (n is equal to N_A in the notation of this article). Normally, to obtain the ASTM grain-size number, at least 50 grains in each of three areas must be counted, the number per square inch must be determined, and this value must be converted to its equivalent at 100×. Then, substitution in Eq 17 or recourse to tables gives ASTM N.

A particularly quick and useful method for determining an equivalent ASTM N uses the P_L count (Ref 20). Provided are two circular test figures of known lengths, as depicted in Fig. 34 (not shown to size). The test circles can be reproduced on plastic sheet (for analyzing photomicrographs) or placed on the ground glass screen of a metallograph. The best method is to use the test circle as a reticle in the focusing eyepiece of a bench microscope.

The operator selects one of the circles and a magnification for the specimen that will result in more than six intersections per application of the circle, on the average. For equiaxed grains that do not vary much in size, the circle is applied to the microstructure until about 35 intersections are obtained, ensuring that a standard deviation of 0.3 units in G, the equivalent grain-size number, is obtained.

To calculate G, the equation is:

$$G = -10.00 - 6.64 \log L_3 \quad \text{(cm)} \qquad \text{(Eq 18)}$$

with:

$$L_3 = \frac{L_T}{PM} \qquad \text{(Eq 19)}$$

where P is the total number of grain-boundary intersections made by a test circle laid down several times to give a total length, L_T (in centimeters), on a field viewed at any magnification, M. To demonstrate the operation of Eq 18, suppose that a 10-cm (4-in.) circle is applied four times to a microstructure at 250×, totaling 36 intersections. G then equals $-10 - 6.64 \log [40/(36 \times 250)]$ or 5.6. Thus, the equivalent grain-size number is obtained directly and efficiently, because no more intersections are counted than required to ensure the desired accuracy. A nomograph for the graphical solution of Eq 18 is reproduced in Fig. 35.

Particle Relationships

Many of the relationships pertaining to particulate structures apply with equal validity to second-phase regions, voids, and boundary precipitates. One important general relationship involves the mean free distance, λ, which is the mean edge-to-edge distance, along random straight lines, between all possible pairs of particles (Ref 1). For α-phase particles, the mean free distance is:

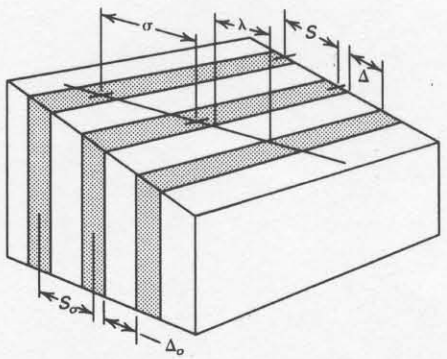

Center-to-center spacings
S_o True spacing
S Apparent spacing
σ Intercept spacing

Edge-to-edge distances
Δ_o True free distance
Δ Apparent free distance
λ Intercept free distance

Fig. 33 Schematic presentation of three types of spacings and three types of distances in a lamellar structure. (Ref 19)

$$\lambda = \frac{1 - (V_V)_\alpha}{N_L} \qquad \text{(Eq 20)}$$

where $(V_V)_\alpha$ is the volume fraction of the α particles and N_L is the number of particle interceptions per unit length of test line. Equation 20 is valid regardless of size, shape, or distribution of the particles and represents a truly three-dimensional interparticle distance. This parameter is important for studies of strength and other mechanical properties and has been used in several different ways as indicated in Fig. 36 and 37.

There are other types of interparticle distance and spacing parameters, such as the mean particle spacing, σ, which is essentially the mean particle center-to-center length. The defining equation for mean particle spacing is:

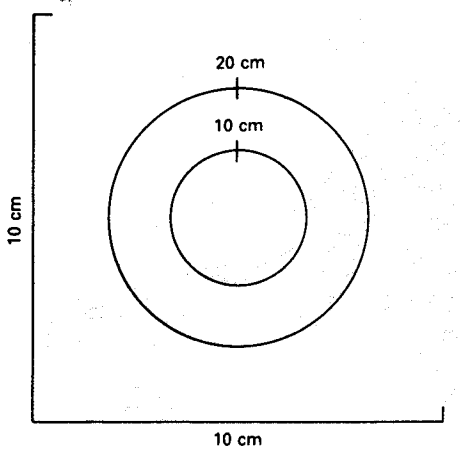

Fig. 34 Hilliard's circular test figures for measurement of grain size. The size of the circles indicated here is suitable for the ground-glass screen of a metallograph.

$$\sigma = \frac{1}{N_L} \qquad \text{(Eq 11a)}$$

where N_L is the number of particle interceptions per unit length of random test lines. The parameter σ is characterized by how easily it can be measured, because only a simple particle interception count is needed. It is also related to λ through the mean intercept length, L_3, by the equation:

$$\lambda = \sigma - (L_3)_\alpha \qquad \text{(Eq 21)}$$

where $(L_3)_\alpha$ for particles of α phase is defined by $(L_3)_\alpha = (L_L)_\alpha / N_L$. This is a general and assumption-free expression, valid for particles of any size or configuration.

The mean particle intercept length, $(L_3)_\alpha$, is a companion term to λ, in that λ is the mean matrix intercept distance and $(L_3)_\alpha$ is the mean particle intercept distance. They are related through the expression for a two-phase or particulate structure of α phase by:

$$\lambda = (L_3)_\alpha \left[\frac{1 - (V_V)_\alpha}{(V_V)_\alpha}\right] \qquad \text{(Eq 22)}$$

where λ is the mean free distance between particles that have a volume fraction $(V_V)_\alpha$ and mean intercept length $(L_3)_\alpha$. Equation 22 has been used to verify the value of volume fraction in a two-phase alloy, such as in Fig. 38. Size and configuration of the dark second phase can be varied readily by heat treatment, but the volume fraction remains relatively constant. Therefore, the (constant) volume fraction obtained from the slope of the curve for λ versus $(L_3)_\alpha$ (73.2 vol%) corresponds well with the volume fractions determined by point counting (73.5 vol%) and from chemical analysis (71.4 vol%).

Note that the mean intercept lengths for space-filling grains and for particles are related through the general expression:

$$L_3 = \frac{L_L}{N_L} \qquad \text{(Eq 23)}$$

In single-phase alloys, L_L (or V_V) = 1, and Eq 16 is obtained. For two-phase or particulate alloys, L_L (or V_V) has a value less than 1, and Eq 23 is used. Also, $2N_L = P_L$ applies to particulate systems, whereas $N_L = P_L$ applies to the single-phase alloys.

An example of the application of the mean intercept lengths is seen in the well-known relationship:

$$R = \frac{4r}{3V_V} \qquad \text{(Eq 24)}$$

where R is the grain radius and r the particle radius. Experimentally, L_3 and $(L_3)_\alpha$ were obtained and used for the grain diameter and particle diameter, respectively; results are shown in Fig. 39. The agreement between calculated and measured grain sizes is considered good.

From the above discussion of grain and particle characteristics, it is evident that there are many points of similarity in their geometrical properties. On the plane of polish, the grain boundaries and particle interphase traces are measured by L_A or L_p (the perimeter length); the intercept distances for both grains and particles are expressed by L_2 or L_3; and the surface area per particle or grain, S/V, and the surface area per unit volume of specimen, S_V, apply equally to both volume elements.

However, because the grains are space filling, all grain boundaries are shared by two contiguous grain faces; particles, on the other hand, do not usually occupy 100% of the alloy. Therefore, sharing of particle boundaries does not occur as often. To emphasize these differences, Table 3 summarizes the pertinent equations for planar figures, area-filling and separated; the same information for grains and particles is in Table 4. In general, the quantities in the second and third columns of each table are double those in the first column, except for the P_L measurements.

The parameters defined in Tables 3 and 4 apply equally to interpenetrating two-phase structures and to simple particulate systems. In one study a series of beryllium-aluminum alloys (similar to the alloy shown in Fig. 38) was investigated for possible correlations between microstructure and mechanical properties. Mechanical properties correlated well with such microstructural quantities as λ, L_3, L_A, and V_V. However, to assess the effects of heat treatment, a new parameter was devised to consider the gradual smoothing of interphase boundaries at higher temperatures. This new parameter, called the "complexity index" (CI), is defined by:

$$\text{CI} = \frac{L_p}{(A)_{\text{Al}}} \qquad \text{(Eq 25)}$$

where L_p, the mean perimeter length of aluminum islands, is equal to $L_A/(N_A)_{\text{Al}}$, and $(A)_{\text{Al}}$, the mean area of aluminum islands is equal to $(A_A)_{\text{Al}}/(N_A)_{\text{Al}}$. Therefore, for the complex, jagged interphase traces, L_p (and CI) is large; however, for smooth, rounded phase areas, L_p (and CI) is small. Dividing by $(A)_{\text{Al}}$ normalizes L_p in terms of the island size. Note that this is not a dimensionless parameter, but has dimensions of reciprocal length.

Plotting the complexity index against elastic modulus, yield strength, hardness, or elongation yields satisfactory correlations of the experimental data. The most striking results are found with the elastic modulus and yield strength of extruded alloys, with and without annealing; typical curves are shown in Fig. 40 for alloys of three compositions. As a result of this type of curve, patent claims were made for alloys with complexity indices between 1 and 5 per micron. Out of 18 claims in Ref 24, seven were based on complexity index and other quantitative microstructural parameters.

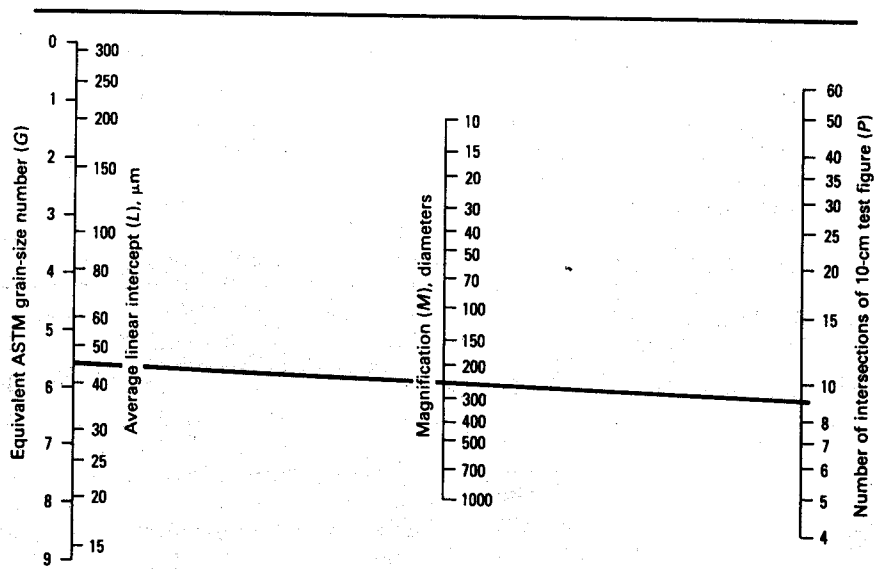

Fig. 35 Nomograph for obtaining ASTM grain-size numbers. (Ref 20)

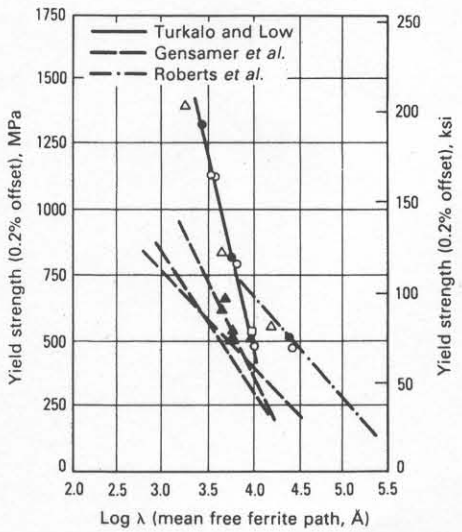

Fig. 36 Yield strength of steels as a function of the mean free distance between cementite particles. (Ref 21)

Particle-Size Distributions

Several methods are available for obtaining the spatial size distribution of spheres from the size distribution of their planar sections. Procedures are also available for convex particles of arbitrary shape (Ref 8), ellipsoids (Ref 25), pentagonal dodecahedrons (Ref 26), a statistical grain shape (Ref 27), and the spacings in lamellar structures (Ref 28). Although the equations for the simpler particles provide statistically exact solutions, this is not the case for size distribution of real particles with irregular shapes. Consequently, assumptions are required, with a corresponding loss in the accuracy of the results.

The three main types of measurements made on planar sections are the section diameters, section areas, or section chords. These are depicted in Fig. 41. From the resulting two-dimensional size distribution, the true spatial size distribution of particles or of grains can be calculated.

Frequently, however, the size-distribution curve is not necessary to characterize a microstructure. In fact, numerical parameters, not a curve, are required to relate the size distribution to some material property. Generally, representing a size-distribution curve requires only the mean diameter, $\bar{D}$, the standard deviation, $\sigma(D)$, and the number of particles per unit volume, N_V. These parameters can be obtained from the analysis of the particle-size distribution or, in some cases, directly from the appropriate experimental data.

A comparison is made in Table 5 of selected methods for obtaining the spatial size distribution of systems of particles with specific shapes. Methods that deal with nonspherical particles are noted, as are those that employ nonanalytical solutions. The unusually simple methods are given in Ref 8 and 29. The procedures involved in the calculations of size distributions will be briefly discussed.

Table 3 Equations for two-dimensional planar figures

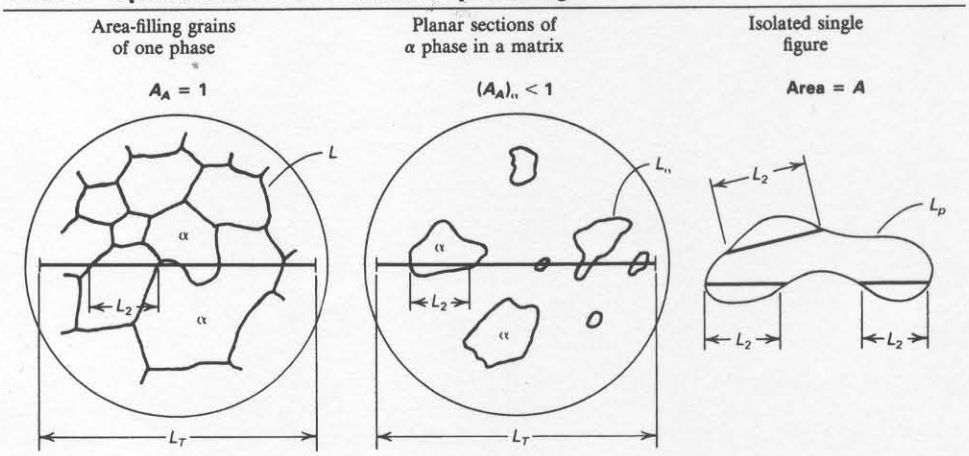

Area-filling grains of one phase	Planar sections of α phase in a matrix	Isolated single figure
$N_L = 1/2 + 4 + 1/2 = 5$	$N_L = 4$	$N_L = 1, 2, \ldots$
$P_L = 5$	$P_L = 8$	$P_L = 2, 4, \ldots$
$P_L = N_L = 1/L_2$	$P_L = 2N_L = 2(A_A)_\alpha / L_2$	$P_L = 2N_L$
Saltykov equations		
$L_A = \frac{\pi}{2} P_L = \frac{\pi}{2} N_L$	$(L_A)_\alpha = \frac{\pi}{2} P_L = \pi N_L$	$\frac{L_p}{A} = \frac{\pi P_L}{2P_P}$
Tomkeieff equations		
$L_2 = \frac{\pi A}{L_p} = \frac{\pi}{2L_A}$	$L_2 = \frac{\pi A_\alpha}{(L_p)_\alpha} = \frac{\pi (A_A)_\alpha}{(L_A)_\alpha}$	$L_2 = \frac{\pi A}{L_p}$
Chalkley equations		
$L_2 = \frac{lh}{2P}$	$L_2 = \frac{lh}{P} = \frac{\pi A_\alpha}{(L_p)_\alpha}$	$L_2 = \frac{lh}{P} = \frac{\pi A}{L_p}$

L_p = mean perimeter length per planar figure = L_A/N_A
L_2 = mean intercept length of planar figures = $L_L/N_L = A_A/N_L$
l = constant length of short test lines, thrown randomly on microstructure
h = number of (end) points of l lines that hit in area of interest
P = number of intersections with perimeters made by l lines
L_T = length of test line

Source: Ref 1

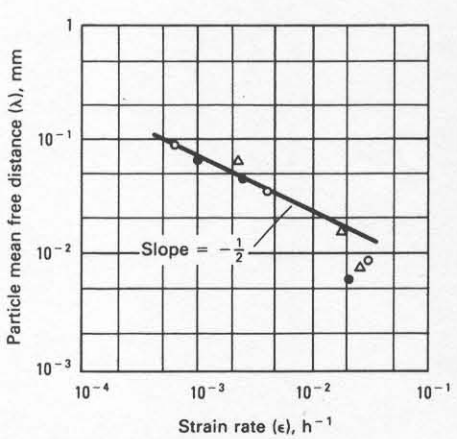

Fig. 37 Strain rate of copper-aluminum dispersion alloys as a function of mean free distance between particles. (Ref 22)

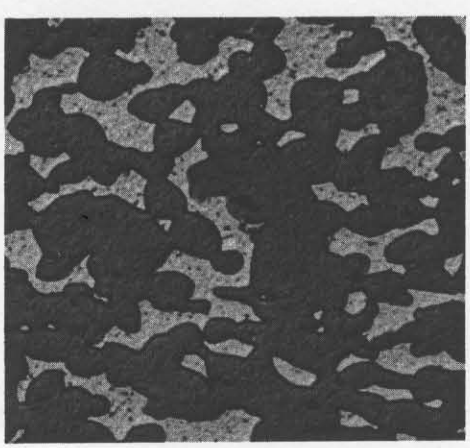

Fig. 38 Interpenetrating two-phase beryllium-aluminum alloy. Etchant and magnification not reported

The first method is based on relative section areas, A/A_{max}, from the planar distribution curve of sections through a sphere. It also applies to any system of convex particles of one shape. A logarithmic scale of diameters is used with the factor $10^{-0.1} = 0.7943$. Therefore, for sectional areas, the factor is $(10^{-0.1})^2 = 0.6310$. Table 6 gives group numbers, the corresponding diameters, and the relative section-area limits required for the class intervals.

Because the section area is specified in

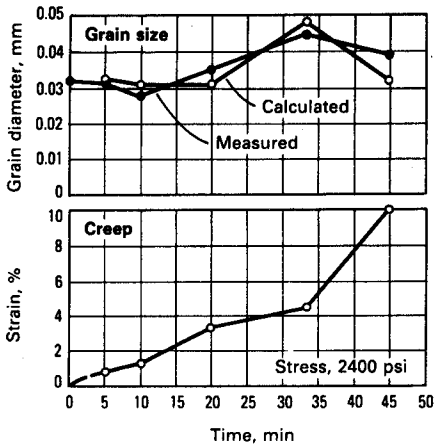

Fig. 39 Comparison of measured and calculated grain size in creep specimens of particulate aluminum-copper alloys. (Ref 23)

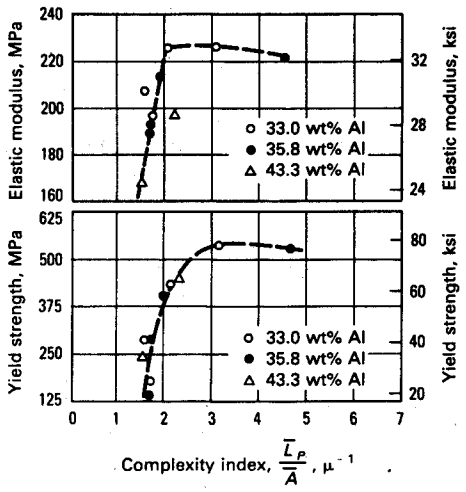

Fig. 40 Elastic modulus and yield strength of three beryllium-aluminum alloys, as functions of complexity index. (Ref 24)

terms of the largest section area, many sections must be examined to obtain the correct volume of A_{max}. Next, the sections per unit area $(N_A)_i$ are counted, then grouped according to the area limits specified in Table 6. A series of graded circles serves this purpose quite well. These values are then substituted in the working equation, which has precalculated coefficients and provisions for 12 class intervals. The equation is:

$$(N_V)_j = \frac{1}{D_j}\Big[1.6461(N_A)_i - 0.4561(N_A)_{i-1} - 0.1162(N_A)_{i-2} - 0.0415(N_A)_{i-3} - 0.0173(N_A)_{i-4} - 0.0079(N_A)_{i-5} - 0.0038(N_A)_{i-6} - 0.0018(N_A)_{i-7} - 0.0010(N_A)_{i-8} - 0.0003(N_A)_{i-9} - 0.0002(N_A)_{i-10} - 0.0002(N_A)_{i-11}\Big] \quad \text{(Eq 26)}$$

where $(N_V)_j$ represents the number of particles per unit volume in the jth class interval, and j is an integer with any value from 1 to 12. The largest particle size corresponds to a value of $j = 1$. The i values for the sections

Table 4 Equations for three-dimensional grains and particles

Space-filling grains of one phase	Dispersed particles of α phase in a matrix	Isolated single particle
$V_V = 1$	$(V_V)_\alpha < 1$	Volume = V
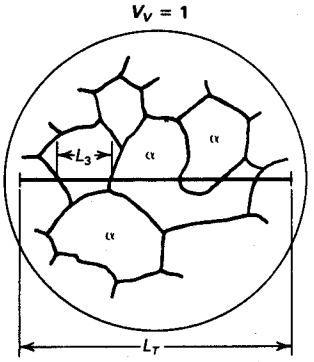	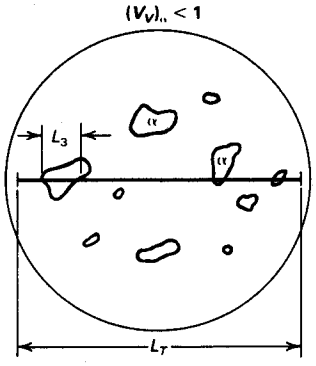	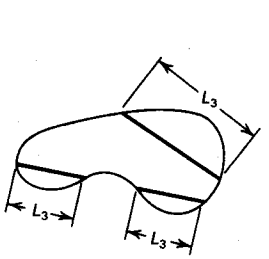
$N_L = 1/2 + 4 + 1/2 = 5$ $P_L = 5$ $P_L = N_L = 1/L_3$	$N_L = 4$ $P_L = 8$ $P_L = 2N_L = 2\,(V_V)_\alpha/L_3$	$N_L = 1, 2, \ldots$ $P_L = 2, 4, \ldots$ $P_L = 2N_L$
Saltykov equations		
$S_V = 2P_L = 2N_L$	$(S_V)_\alpha = 2P_L = 4N_L$	$\frac{S}{V} = \frac{2P_L}{P_P}$
Tomkeieff equations		
$L_3 = 2\frac{V}{S} = \frac{2}{S_V}$	$L_3 = \frac{4V_\alpha}{S_\alpha} = \frac{4(V_V)_\alpha}{(S_V)_\alpha}$	$L_3 = 4\frac{V}{S}$
Chalkley equations		
$L_3 = \frac{lh}{2P}$	$L_3 = \frac{lh}{P} = \frac{4V_\alpha}{S_\alpha}$	$L_3 = \frac{lh}{P} = \frac{4V}{S}$

S_α = mean surface area of α particles = $(S_V)_\alpha/N_V$
L_3 = mean intercept length of three-dimensional bodies = $L_L/N_L = A_A/N_L = V_V/N_L$
l = constant length of short test lines, thrown randomly on microstructure
h = number of (end) points of l lines that hit in phase of interest
P = number of intersections with surfaces made by l lines
L_T = length of test line

Source: Ref 1

Table 5 Comparison of methods for obtaining size distribution of particles with specific shapes

Method	Particle shape	Characteristics of method(a)	Remarks
Diameters			
DeHoff	Ellipsoids	T, I	Uses axial ratios; shape factors obtained from curves
Scheil and Wurst	Statistical grain shape	T, S	Based on ingot iron grains
Schwartz-Saltykov	Sphere	T, I	...
Paulus	Pentagonal dodecahedron	T, C, L, S	Method based on d/d_{max} distribution curve
Areas			
Saltykov	Spheres, convex particles	WE, I, L	Method based on A/A_{max} distribution curve
Chords			
Lord and Willis	Sphere	G, I	...
Cahn and Fullman	Lamellar structures	G, I	Slopes taken from experimental distribution curve
Bockstiegel	Sphere	WE, I, L	No coefficients required in simplified version

(a) T = table of coefficients required; G = graphical method of solution; WE = only working equation needed; C = curve comparison method available; I = independent calculation of each class interval; S = sequential calculations required; L = logarithmic scale

depend on the particular sphere size, or j value, chosen for calculation. Therefore, as each value of j is selected, i is set equal to j; this determines the number of terms used inside the brackets. For example, to calculate the value of $(N_V)_5$, the first five terms in the brackets would be used: for $i = 5$, $i - 1 = 4$, $i - 2 = 3$, $i - 3 = 2$, and $i - 4 = 1$.

To show how the calculations are made, $(N_V)_4$ will be determined from the data given in Table 7. The equation obtained in this case for $j = 4$ $(= i)$ is:

$$(N_V)_4 = \frac{1}{D_4}\Big[1.6461(N_A)_4 - 0.4561(N_A)_3 - 0.1162(N_A)_2 - 0.0415(N_A)_1\Big] \quad \text{(Eq 27)}$$

Substituting the experimental data,

$$(N_V)_4 = \frac{1}{0.0316}\Big[1.65(230) - 0.456(253) - 0.116(161) - 0.0415(104)\Big] = 7630 \text{ mm}^{-3} \quad \text{(Eq 28)}$$

is obtained. This type of calculation would be performed for all particle sizes, and the total would give N_V, the total number of particles per unit volume. The results from the calculations are summarized in Table 8. This method is simple and useful. Of further interest is the possibility of analyzing systems of convex particles of more complex shape.

Table 6 Limits for grouped planar sections from spheres

Group	Relative section diameter, d/d_{max}	Relative section area, A/A_{max}
1	1.0000	1.0000-0.6310
2	0.7943	0.6310-0.3981
3	0.6310	0.3981-0.2512
4	0.5012	0.2512-0.1585
5	0.3981	0.1585-0.1000
6	0.3162	0.1000-0.0631
7	0.2512	0.0631-0.0398
8	0.1995	0.0398-0.0251
9	0.1581	0.0251-0.0158
10	0.1259	0.0158-0.0100
11	0.1000	0.0100-0.0063
12	0.0794	0.0063-0.0040

Table 7 Measured distribution of ferrite grain section sizes

Class interval	Range of section diameters, d_j, mm	Relative section area A/A_{max}	Sections per mm², $(N_A)_i$
1	0.0631-0.0501	1.0000-0.6310	104
2	0.0501-0.0398	0.6310-0.3981	161
3	0.0398-0.0316	0.3981-0.2512	253
4	0.0316-0.0251	0.2512-0.1585	230
5	0.0251-0.0199	0.1585-0.1000	138
6	0.0199-0.0158	0.1000-0.0631	69
N_A, per mm²			955

Table 8 Calculated distribution of ferrite grain sizes

Class interval	Diameter of particles, D_j, mm	No. of grains per mm³, $(N_V)_j$
1	0.0631	2713
2	0.0501	4341
3	0.0398	8313
4	0.0316	7630
5	0.0251	3359
6	0.0199	491
N_V, per mm³		26 847

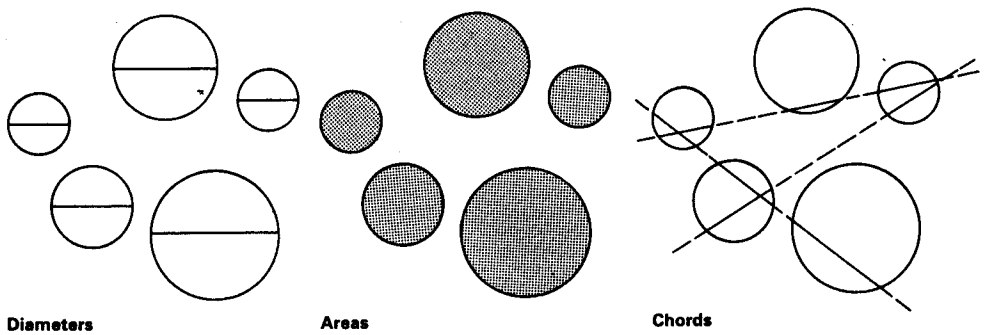

Fig. 41 Schematic presentation of three main types of measurements (diameters, areas, and chords) made on planar sections. (Ref 1)

It may be useful to express the size distribution in terms of the three numerical parameters $\overline{D}$, $\sigma(D)$, and N_V, instead of the size-distribution curve itself. The mean diameter is expressed by:

$$\overline{D} = \frac{1}{N_V}\sum_j (N_V)_j D_j \quad \text{(Eq 29)}$$

the standard deviation by:

$$\sigma(D) = \left[\overline{D_j^2} - \overline{D^2}\right]^{1/2} \quad \text{(Eq 30)}$$

and the total number of particles per unit volume by:

$$N_V = \sum_i^j (N_V)_j \quad \text{(Eq 31)}$$

Therefore, from the data in Table 8, $\overline{D} = 0.0393$ mm, $\sigma(D) = 0.012$ mm, and $N_V = 27\,000$ mm^{-3}. An alternative is to plot the cumulative percentages of $(N_V)_j$ versus particle diameter on log probability graph paper. If the size distribution conforms to the log normal distribution, as most particle and grain-size distributions do, a straight line will result. Then the values of $\overline{D}$ and $\sigma(D)$ can be read from the curve—$\overline{D}$ at a cumulative frequency of 50, and $\sigma(D)$ between 84.13 and 50 or between 50 and 15.87.

Another method for obtaining a particle-size distribution involves measuring the intercept chord-length distribution (Ref 1). Considering ease of data gathering, the chord methods are quite promising, especially since the advent of electronic scanning devices. An improved derivation of the chord-intercept relationship for spheres is given in Ref 29. The number of chords per unit length, $(n_L)_i$, $(n_L)_{i+1}$, and so on, are obtained experimentally and grouped into suitable class intervals, l_{i-1} to l_i, l_i to l_{i+1}, and so on, respectively. To obtain $(N_V)_{i+1/2}$, which represents the number of particles per unit volume with diameters between $l_{i-1/2}$ and $l_{i+1/2}$, the general equation is:

$$(N_V)_{i+1/2} = \frac{4}{\pi}\left[\frac{(n_L)_i}{l_i^2 - l_{i-1}^2} - \frac{(n_L)_{i+1}}{l_{i+1}^2 - l_i^2}\right] \quad \text{(Eq 32)}$$

which is valid for any class-interval division. Note that N_V can be obtained independently for any size group and that tables of coefficients are not required.

A further simplification of Eq 32 is possible by defining logarithmic class intervals such that $l_{i+1} = zl_i$. Putting $z = \sqrt{2}$ gives $l_{i+1}^2 = 2l_i^2$, $l_i^2 = 2l_{i-1}^2$, and so on, which, when inserted into Eq 32 gives:

$$(N_V)_{i+1/2} = C\frac{2(n_L)_i - (n_L)_{i+1}}{(2)^i} \quad \text{(Eq 33)}$$

where $C = 4/\pi\, l_0^2$ and is a constant independent of i, and l_0 is the upper limit of the lowest class interval. If relative values, $(N_V)_{i+1}/\Sigma(N_V)_{i+1/2}$, are desired rather than absolute numbers, $(N_V)_{i+1/2}$, constant C cancels out. Therefore, the relative size distribution is obtained from the experimental data.

As an example of the application of Eq 32,

Table 9 Properties of a sphere, truncated octahedron, and convex particles

Property	Sphere, $D = 2r$	Truncated octahedron, edge length $= a$	General equations for convex particles
V	$4\pi r^3/3$	$11.314a^3$	$V = A'L_3 = AH'$
S	$4\pi r^2$	$26.785a^2$	$S = 4A' = 4V/L_3$
A'	πr^2	$6.696a^2$	$A' = S/4 = V/L_3$
H'	$2r$	$3.0a$	$H' = V/A = A'L_3/A$
A	$2\pi r^2/3$	$3.77a^2$	$A = V/H' = A'L_3/H'$
L_3	$4r/3$	$1.69a$	$L_3 = 4V/S = AN_A/N_L$
r, a, ρ(a)	$r = 2N_L/\pi N_A$	$a = 0.45N_L/N_A$	$\rho = H'/2 = N_A A'/2N_L = A'/2L_3'$
N_V	$\pi N_A^2/4N_L$	$0.744N_A^2/N_L$	$N_V = N_A/H' = N_L/A'$

General equation: $V_V = N_V V = N_A A = N_L L_3$

(a) ρ = half of mean tangent diameter
Source: Ref 1

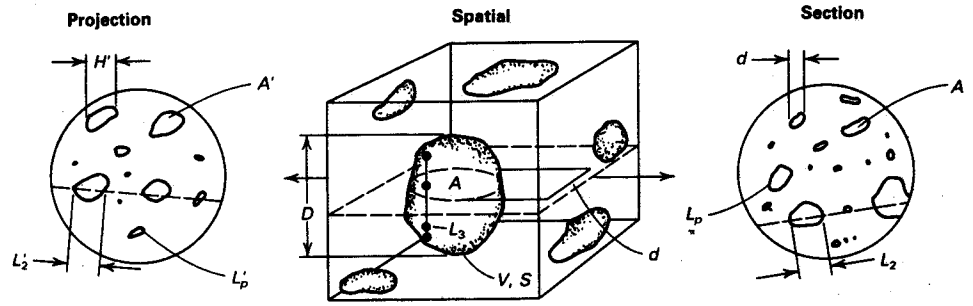

$A' = L_2' \cdot H'$ $\quad N_L' = N_A' \cdot H'$ $\quad V = A \cdot D = A' \cdot L_3$ $\quad L_3 = 4V/S$ $\quad A = L_2 \cdot d$ $\quad N_L = N_A \cdot d$

$L_2' = \pi A'/L_p'$ $\quad L_2' = d$ $\quad S = 4A'$ $\quad D = H'$ $\quad L_2 = \pi A/L_p$ $\quad N_A = N_V \cdot D$

$H' = L_p'/\pi$ $\quad H' = A'/d'$ $\quad A = L_3 \cdot L_2'$ $\quad L_3 = L_2$ $\quad d = L_p/\pi$ $\quad N_V = N_L/A'$

Fig. 42 Relationships among convex particles in space, their sections, and their projections (projected quantities are indicated by primes)

consider the case for $i = 4$ given the following data:

Group	Range of chord lengths, mm	Chords per mm, $(N_L)_i$	Diameters of particles, mm
4	0.0075-0.0100	19	0.0100
5	0.0100-0.0125	13	0.0125

Substitution in Eq 32 gives:

$$(N_V)_{i+1/2} = \frac{4}{\pi}\left[\frac{19}{(10^2 - 7.5^2)10^{-6}} - \frac{13}{(12.5^2 - 10^2)10^{-6}}\right]$$

$$= \frac{4}{\pi}\left[\left(\frac{19}{43.75} - \frac{13}{56.25}\right)10^6\right]$$

$$= 259\,000 \text{ mm}^{-3}$$

Calculation at $i = 4$ according to Eq 33 results in:

$$(N_V)_{i+1/2} = C\left[\frac{(2 \times 19) - 13}{(2)^4}\right] = C\left(\frac{25}{16}\right)$$

$$= C(1.56)$$

This result would be divided by $\Sigma(N_V)_{i+1/2}$ to obtain the relative particle frequency at $i = 4$. Occasionally, negative values are obtained for the smallest particles. Reasons for this are discussed in Ref 1. A practical solution is to equate the negative values to zero.

Projected Images

In general, microscopists encounter two types of projected images. In the first, the image results from a transmitted beam through the specimen, representing the features located within the three-dimensional space (such as by thin-foil transmission electron microscopy). In the second, the projected image is generated by a reflected beam from the external surface of the specimen (such as by scanning electron microscopy).

Only the most rudimentary quantitative calculations can be made on images projected by the reflection techniques (Ref 30). In rough surfaces, the intensity levels depend on topography, and some features may be masked by others. Three-dimensional characterization is based on the photogrammetric analysis of stereopairs, for which automatic image-analyzing techniques are not yet available (Ref 31).

Quantitative statistical treatment of transmitted-beam images, however, has matured to a much greater extent. These analyses (Ref 32, 33) are too lengthy and complex to be treated here, but are described in the literature (see Ref 1).

One final topic will be included, because of its importance to the analysis of particulate systems. Figure 42 provides interrelated general equations of convex particles that express the important spatial parameters in terms of measurements made on the plane of polish and the projection plane. Application of the equations to specific particles is summarized in Table 9 for the sphere, for the truncated octahedron (or tetrakaidecahedron), and for convex particles in general. Tabulations of the type presented in Table 9 permit the microscopist to approximate microstructures with particles of known shape when other techniques are not feasible.

REFERENCES

1. E.E. Underwood, *Quantitative Stereology*, Addison-Wesley, 1970
2. J.E. Hilliard and J.W. Cahn, *Trans. Met. Soc. AIME*, Vol 221, 1961, p 344
3. J.E. Hilliard, in *Quantitative Microscopy*, R.T. DeHoff and F.N. Rhines, Ed., McGraw-Hill, 1968, p 72
4. "Standard Methods for Estimating the Average Grain Size of Metals," E 112, *Annual Book of ASTM Standards*, Vol 03.03, ASTM, Philadelphia, 1984, p 120
5. W.T. Pell-Walpole, *J. Inst. Metals*, Vol 69, 1943, p 131
6. H.W. Chalkley, J. Cornfield, and H. Park, *Science*, Vol 110, Sept. 23, 1949, p 295
7. E.R. Weibel, *Lab. Invest.*, Vol 12 (No. 2), 1963, p 131
8. S.A. Saltykov, in *Stereology*, H. Elias, Ed., Springer-Verlag, 1967
9. S.A. Saltykov, *Stereometric Metallography*, 3rd ed., Metallurgizdat, Moscow, 1970 (in Russian)
10. M.G. Kendall and P.A.P. Moran, *Geometrical Probability*, No. 10, Griffin's Statistical Monographs and Courses, C. Griffin and Co., Ltd., London, 1963
11. E.R. Weibel, *Morphometry of the Human Lung*, Springer-Verlag, 1963
12. B.I. Edelson and W.M. Baldwin, Jr., *Trans. ASM*, Vol 55, 1962, p 238
13. L.H. Beck and C.S. Smith, *Trans. AIME, Inst. Metals Div.*, Vol 194, 1952, p 1079
14. *Deformation Twinning*, R.E. Reed-Hill *et al.*, Ed., Gordon and Breach, 1964
15. J.B. Newkirk and J.H. Wernick, Ed., *Direct Observations of Imperfections in Crystals*, Interscience, 1962
16. S. O'Hara, *J. Appl. Phys.*, Vol 35, 1964, p 409
17. A.S. Yue, *Trans. Met. Soc. AIME*, Vol 224, 1962, p 1010
18. J. Nutting and R.G. Baker, *The Microstructure of Metals*, Monograph and Report Series No. 30, Institute of Metals, London, 1965, p 53
19. R.M. Fulrath and J.A. Pask, Ed., *Ceramic Microstructures*, John Wiley & Sons, 1968, p 48
20. J.E. Hilliard, *Met. Prog.*, Vol 85, May 1964, p 99
21. A.M. Turkalo and J.R. Low, Jr., *Trans. Met. Soc. AIME*, Vol 212, 1958, p 757
22. R.W. Guard in *Strengthening Mechanisms in Solids*, American Society for Metals, 1962, p 274
23. E.E. Underwood and G.K. Manning, *Mem. Sci. Rev. Met.*, Vol 60 (No. 9), 1963, p 648
24. U.S. Patent No. 3,337,334, Aug 22, 1967
25. R.T. DeHoff, *Trans. Met. Soc. AIME*, Vol 224, 1962, p 474
26. M. Paulus, *Metaux (Corrosion-Ind.)*, Vol 37 (No. 448), Dec 1962, p 447; Vol 38 (No. 449), Jan 1963, p 14; Parts I and II
27. E. Scheil and H. Wurst, *Z. Metallk.*, Vol 28 (No. 11), 1936, p 340
28. J.W. Cahn and R.L. Fullman, *Trans. AIME, Inst. Metals Div.*, Vol 206, 1956, p 610
29. G. Bockstiegel, *Z. Metallk.*, Vol 57, 1966, p 647
30. J.E. Hilliard, *J. Microsc.*, Vol 95 (Part 1), Feb 1972, p 45-58
31. T.O. Johari, *Res. Develop.*, Vol 22 (No. 7), 1971, p 12
32. E.E. Underwood, The Stereology of Projected Images, *J. Microsc.*, Vol 95 (Part 1), Feb 1972, p 25-44
33. E.E. Underwood, The Mathematical Foundations of Quantitative Stereology, in *Stereology and Quantitative Metallography*, STP 504, ASTM, Philadelphia, 1972, p 3-38